ACS APPLIED MATERIALS & INTERFACES

Research Article

www.acsami.org

Tailoring Polyacrylonitrile Interfacial Morphological Structure by Crystallization in the Presence of Single-Wall Carbon Nanotubes

Yiying Zhang, Kenan Song, Jiangsha Meng, and Marilyn L. Minus*

Northeastern University, Department of Mechanical and Industrial Engineering, College of Engineering, 360 Huntington Avenue, 334 Snell Engineering Center, Boston, Massachusetts 02115-5000, United States

ABSTRACT: In order to improve stress transfer between polymer matrixes and nanofillers, controlling the structure development in the interphase region during composite processing is a necessity. For polyacrylonitrile (PAN)/single-wall carbon nanotubes (SWNT) composites, the formation of the PAN interphase in the presence of the SWNT as a function of processing conditions is studied. Under these conditions, three distinct interfacial coating morphologies of PAN are observed on SWNT. In the semidilute polymer concentration regime subjected to shearing, PAN extended-chain tubular coatings are formed on SWNT. Dilute PAN/SWNT quiescent solutions subjected to cooling yields hybrid periodic shish-kebab structures (first observation for PAN polymer), and dilute PAN/SWNT quiescent solutions subjected to rapid cooling results in the formation of an irregular PAN crystalline coating on the SWNT.

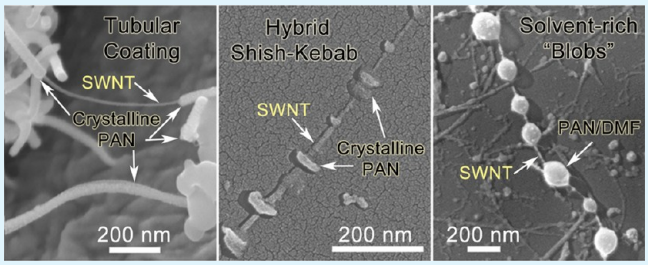

KEYWORDS: *interphase, crystallization, polyacrylonitrile, SWNT, extended-chain, shish-kebab*

1. INTRODUCTION

Carbon nanotubes (CNT), known for their unique geometrical shape and extremely strong properties,[1−3] have already been utilized to reinforce several polymer-based nanocomposites.[4−7] However, the nanocomposite properties to date are still significantly lower than what have been theoretically predicted and/or expected. Mechanical property improvement in nanocomposite materials is to a great extent attributed to the formation of the polymer−CNT interphase,[8,9] which improves the interfacial interactions and stress transfer between the matrix and CNT. Control over the interphase structure formation can improve polymer wetting behavior, adhesion, and load transfer[10−12] and, in turn, dictate the properties of the macroscopic composite.[13,14] Other contributing factors to the mechanical properties include the CNT aspect ratio, loading, and exfoliation in the polymer matrix. These factors may also affect the quality and quantity of the polymer interphase formation in the nanocomposite.

For high-performance polymer-based CNT fibers, it has been shown that increasing the amount of crystalline polymer interphase improves CNT-to-matrix load transfer even with low CNT loading.[5,7,9] It should also be noted that these interfacial regions have been observed in high-performance polymer/CNT fibers with low loading of CNT (i.e., on the order of 1 wt %).[5−7,15] Therefore, it is reasonable to assume that, by improving the interphase structure and in particular increasing in the amount of the crystalline polymer interphase, the composite properties would be significantly improved. Integrating interphase growth with current processing technologies for nanocomposites also enables the fabrication of ultrastrong and inexpensive materials that utilize low CNT loading (i.e., < 1 wt %).

These crystalline polymer interphase structures are a result of the CNT acting as a template. For this reason, CNT templated interfacial crystallization is one route to control the polymer interphase formation.[6] Previous work has shown that single-wall carbon nanotubes (SWNT) can template extended-chain polymer crystallization in both polyacrylonitrile (PAN) and poly(vinyl alcohol) (PVA) systems.[5−7,15] CNT can also nucleate periodic folded-chain lamellar crystals (i.e., known as a hybrid shish-kebab structure) for polyethylene (PE),[16−20] nylon 6,6,[17] PVA,[21] poly(butylene terephthalate) (PBT),[22−24] isotactic polypropylene (iPP),[25] poly(L-lactide) (PLLA),[25] and polyethylene-*b*-poly(ethylene oxide) (PE-b-PEO) block copolymer.[26] The mechanism of carbon-induced crystallization in some cases can be attributed to polymer epitaxial interactions with the hexagonal graphite surface. This refers to the polymer crystallizing in registry with the graphitic substrate due to crystal lattice matching. Researchers have explored polymer epitaxial crystallization on graphitic substrates with various geometries, such as flat surfaces of graphite[27−30] or graphene oxide nanosheets,[16,31] curved surfaces of carbon fibers,[32,33] and highly curved surfaces of CNT materials.[5−7,16,34,35]

For polymeric materials, extensional force (usually conducted through shear flows in melt or solution) is required for inducing the extended-chain crystallization and the subsequent growing of the bundle-like fibrils.[36,37] This shearing mechanism

Received: October 18, 2012
Accepted: January 3, 2013
Published: January 3, 2013

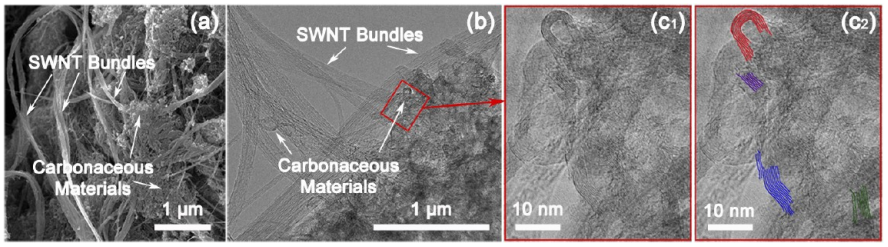

Figure 1. As-received SWNT powder showing the presence of the SWNT bundles as well as other carbonaceous particles (a) scanning electron micrograph and (b) transmission electron micrograph. (c_1) High-resolution transmission electron micrograph showing the graphitized structures of the carbonaceous materials. For (c_2), a schematic is included to identify the area where graphitic planes can be clearly observed.

is also needed to grow fibrillar (extended-chain) crystals in polymer−nano hybrid systems.[5−7,18] CNT have been shown to induce nucleation and orientation of extended-chain crystallization.[5−7,18] The extended-chain polymer conformation is the most desired structure for fabricating strong fibers with both high modulus and strength. On the basis of theoretical calculations, it is shown that the moduli for some thermoplastic polymers in the extended-chain conformation are significantly higher than current commercial materials made utilizing these polymers. Examples include PVA at 255 GPa, PE at 240 GPa, and polytetrafluoroethylene (PTFE) at 156 GPa.[38] Therefore, the potential for producing high-performance fibers from typical thermoplastic polymer materials is very high.

Interfacial crystallization of PAN with SWNT was studied in this work. The interfacial structure in PAN/SWNT composites has been shown to directly affect stress transfer properties and the ultimate mechanical performance.[5,15] PAN is the most widely used precursor polymer for carbon fiber production. The next-generation of PAN-based carbon fibers are being researched, where PAN/SWNT-based fibers are being studied as precursor fiber materials.[4] These next-generation carbon fibers from PAN/SWNT gel-spun precursor fibers exhibit crystalline interface regions.[4,5] It was observed that the crystalline interfacial PAN could be graphitized at low carbonization temperature (∼1100 °C) due to SWNT templating of the PAN molecules.[15] For this reason, understanding the interphase polymer development in the PAN/SWNT system is of significant importance.

This research also shows that, using specific temperature control (i.e., degree of undercooling (ΔT), initial solution temperature (T_o) − final solution temperature (T_f)), solution concentration, and shearing processes for PAN/SWNT mixtures, tailored interphase structures could be formed. In the vicinity of SWNT, uniform tubular coating of PAN (extended-chain) was formed under shear at the relatively high crystallization temperature and concentration. In dilute solutions undergoing quiescent cooling, the first observation of PAN/SWNT shish-kebab structure (i.e., PAN kebab structure (folded-chain) on SWNT shish) was shown. In addition, an irregular coating of PAN was also formed on SWNT by quenching quiescent dilute PAN/SWNT solutions.

2. EXPERIMENTAL SECTION

2.1. Materials. PAN (molecular weight, ∼520 000 g mol^{-1}) was obtained from Japan Exlan Co. SWNT powder was obtained from Cheaptubes Inc. (Cat. # SKU-0101; CVD synthesized; purity, >90 wt %; average diameter, 1−2 nm). On the basis of scanning electron microscopy and transmission electron microscopy analysis, it was found that in addition to SWNT the Cheaptube samples contain other carbonaceous species (i.e., onions and carbon black) (Figure 1). Raman curves for the SWNT sample show only a small D-band peak (disorder band), where the intensity of the G-band ($I_{G\text{-band}}$) is ∼45 times higher in magnitude than the intensity of the D-band ($I_{D\text{-band}}$). *N*,*N*-Dimethylformamide (DMF) (≥99.8%) solvent was purchased from Sigma-Aldrich (CAS# 68-12-2) and used as-received.

2.2. Solution Preparation. As-received SWNT powder was added into a dilute PAN/DMF solution held at 90 °C. The PAN/SWNT/DMF mixture was immediately transferred to a sonication bath initially held at 90 °C for dispersion. Bath sonication was conducted using a Fisher F530 bath sonicator (frequency, 43 kHz; power, 150 W). PAN/SWNT/DMF solutions with different concentrations were prepared in three procedures. Table 1 summarizes the concentration, processing methods, and range of solution temperatures for Solution-a_1 (S-a_1), Solution-a_2 for comparison (S-a_2), Solution-b (S-b), and Solution-c (S-c). The samples are classified on the basis of processing conditions (Figure 2) and SWNT concentrations (Table 1).

Table 1. Solution Processing and Crystallization Conditions Used to Grow the Various Interphase Structures of PAN on SWNT

processing parameters			solution batches			
			S-a_1	S-a_2	S-b	S-c
concentration of SWNT		(mg L^{-1})	250	20	20	20
concentration of PAN		(mg L^{-1})	250	20	20	20
		(wt %)	25	2	2	2
PAN/SWNT solution processing stages	(1) sonication conditions		time: 24 h; bath temperature range: 55−90 °C			
	(2) postprocessing (i.e., shearing)		4 h stirring at 90 °C		none	none
	(3) cooling	initial (T_o) (°C)	90	90	∼55	∼55
		final (T_f) (°C)	60	60	20	20
		cooling rate (°C/min)	4	4	2	29
degree of undercooling ($\Delta T = T_o - T_f$) (°C)			30	30	70	70

Figure 2 shows the processing conditions used to grow PAN interfacial structure on SWNT from the various PAN/SWNT solutions. The PAN/SWNT solutions were put through three major steps: (1) sonication (to improve PAN/SWNT dispersion), (2) a postprocessing shearing step (to induce fibrillar crystal nucleation), and (3) a cooling stage (to induce polymer crystallization). All PAN/SWNT solutions were sonicated for 24 h. The sonication bath was temperature controlled within the range of 90−55 °C. S-a samples were the only ones subjected to a postprocessing (shearing) step (Figure 2). Both S-a_1 and S-a_2 samples were cooled to 60 °C and vacuum-dried at this temperature before analysis. For the S-b samples, the original sonicated solution was diluted to 20 times the original volume with DMF at solution temperature (T_o) (Figure 2 (S-b)) before cooling to room temperature (20 °C). S-c samples were diluted to 20 times the original volume with room temperature (20 °C) DMF.

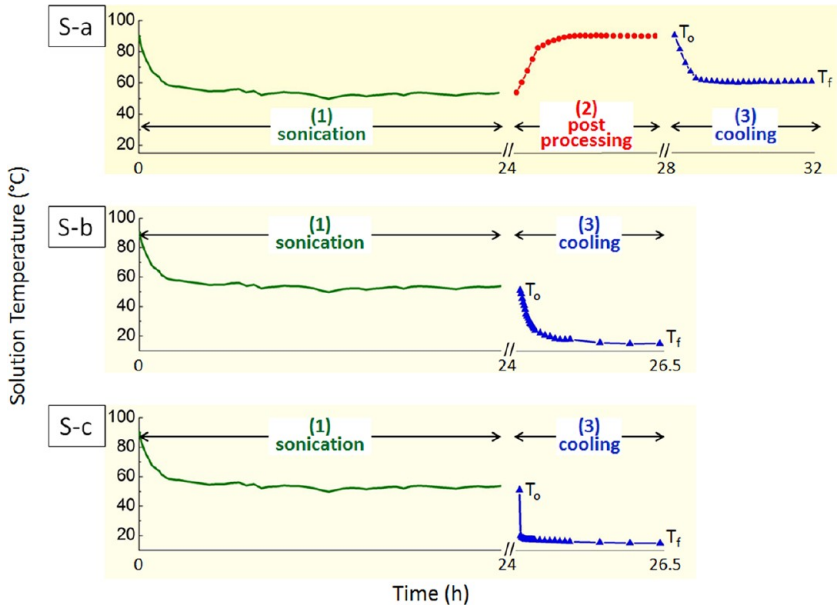

Figure 2. Graphical representation of the solution temperature change as a function of processing time for the PAN/SWNT solutions. All solution processing stages ((1) sonication, (2) postprocessing, and (3) cooling) were temperature controlled. Table 1 lists the specifications for each processing stage.

The diluted S-c samples were allowed time to equilibrate to ~20 °C before being taken for analysis. All samples were vacuum-dried (at temperatures ranging from 25 to 90 °C) on polished silicon wafers for SEM observation.

2.3. Sample Characterization. Morphology characterization was performed on a Zeiss Supra 25 field emission scanning electron microscope (SEM) (operating voltage, 5 kV) and Helios Nanolab 600 dual beam focused ion beam milling system (operating voltage, 5 kV). All samples were sputter coated with gold/palladium for image analysis by scanning electron microscopy. Wide-angle X-ray diffraction was performed on a Rigaku RAPID II curved detector X-ray diffraction (XRD) system equipped with a 3 kW sealed tube source (voltage, 40 kV; current, 30 mA). XRD curve fitting and analysis was performed using software's PDXL 2 (version 2.0.3.0) and 2DP (version 1.0.3.4). For X-ray analysis, thin PAN/SWNT buckypaper-like samples were prepared by drying the PAN/SWNT samples in a vacuum oven. Transmission electron microscopy was performed on a JEOL 2010 advance high performance transmission electron microscope (TEM) (operating voltage, 200 kV). TEM samples were prepared using loop tool (electron microscopy sciences cat. # 70944) to place droplets of the PAN/SWNT dispersion onto lacey carbon coated copper grids (electron microscopy sciences cat. # LC200-Cu). Lattice measurements from TEM were calibrated and verified using a graphitized carbon black (electron microscopy sciences cat. # 80037) standard.

3. RESULTS AND DISCUSSION

As a result of tailoring the processing parameters, various interfacial PAN coating structures were formed on SWNT (Table 1). By comparing these various PAN morphologies, it was found that PAN/SWNT solutions with high PAN concentration (S-a_1) slow cooled under shear force (Figure 2 (S-a)) resulted in the formation of extended-chain crystals at the PAN/SWNT interphase. Lower PAN concentration with slow cooled quiescent PAN/SWNT solutions led to the formation of hybrid PAN/SWNT shish-kebab structures (Figure 2 (S-b)). This is the first observation of shish-kebab structures in the PAN polymer system. In addition, at low PAN concentration, quiescent PAN/SWNT solutions subjected to fast cooling (quenching) resulted in the formation of PAN/DMF "blobs" on the SWNT bundles (Figure 2 (S-c)). Subsequent removal of the solvent by heat drying resulted in irregular lamellar growth of PAN on the SWNT (see Section 3.2.1).

Inherently, it is more difficult for helical polymers to epitaxially crystallize on CNT as compared to polymer with planar zigzag conformations.[19] This is due to the reduction of regularity and contacting density caused by less symmetry of the helix as well as the presence of bulky side groups.[39] Previous studies have shown that lamellar single crystals of PAN have been grown in various solvents. These crystals have been characterized by electron microscopy.[40] There has been some debate over the *c*-axis (chain axis) unit cell length for PAN. However, it is generally believed that the lamellar single crystal observed consists of folded chains, since the thickness is much less than the chain contour length. The observation of interfacial crystalline PAN coated on SWNT in this work shows the evidence that PAN (helical conformation) can form both extended-chain (tubular coating) and folded-chain (kebabs) crystalline structures nucleated by SWNT, under appropriate crystallization conditions. Wide-angle X-ray diffraction (WAXD) for these samples (Figure 3) confirms the PAN crystalline structure of the coatings.

As previously mentioned, the presence of interfacial structure in PAN/SWNT-based gel-spun fibers greatly improves its mechanical performance.[5] This is due to better stress transfer between the PAN matrix and SWNT. It should be mentioned that the sonication processing time, temperatures, and shearing conditions used in this work to grow the various interfacial coatings are similar to those used in the typical gel-spinning procedures for PAN/SWNT fibers. For example, a typical gel-spun PAN/SWNT composite fiber is produced by processes including (i) SWNT dispersion, (ii) polymer dope preparation, and (iii) fiber spinning. During these processes, PAN will experience changes in solution temperature, concentration, and shear forces, which may cause different interfacial crystallization processes to occur during fabrication. This work shows that, over a broad temperature range (i.e., 90 to 20 °C), polymer concentration, and processing procedures, multiple types of

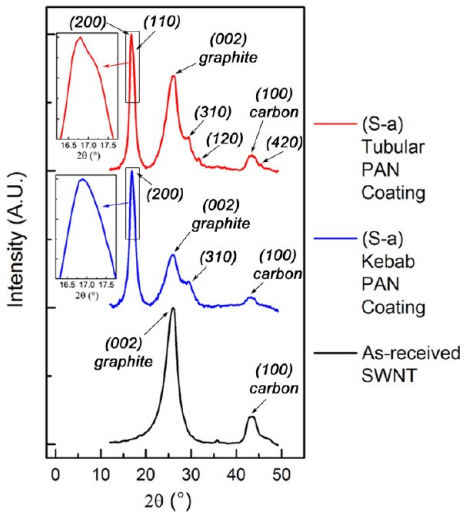

Figure 3. Wide-angle X-ray diffraction 2θ versus intensity curves for (S-a) tubular PAN and (S-b) kebab PAN coated SWNT, as well as as-received SWNT. Insets show a magnification of the PAN major peak.

interfacial structures can be formed. The presence of these various interfacial structures within a macroscopic composite will no doubt cause variations in stress transfer mechanisms at the interphase. In addition, lack of control over the processing parameters may also affect the consistency of morphology and structural formation in the macroscopic composites. For composites produced at the lab-scale in batch-to-batch processes, this will inevitably translate to significant variations in the mechanical properties. This study brings to light the specificity required for processing conditions of nanocomposite systems in order to control the type of interfacial structure present. In the sections below, the conditions for the formation for each type of PAN interfacial coating and its structure are discussed in more detail.

3.1. Uniform Tubular Coating. Figure $4a_1-a_3$ shows that PAN forms a very uniform tubular coating around the SWNT bundles. Figure 3 shows the WAXD 2θ versus intensity profile for these materials. The X-ray results show PAN (200), (110), (310), (120), and (420) peaks in addition to two broad peaks associated with the carbonaceous species in the SWNT sample (i.e., (002) graphite peak and (100) carbon peak at ~26° and ~42°, respectively (Figure 3)). Indexing for PAN was determined assuming an orthorhombic PAN unit cell with lattice parameters of a = 1.06 nm, b = 0.58 nm, and c = 0.51 nm.[40,41] Table 2 lists the 2θ, d-spacing, and the crystal sizes of all peaks observed. It should be noted that for these PAN/SWNT samples with tubular coating the major PAN WAXD peak exhibits a distinct shoulder due to the existence of a (200)/(110) doublet, which is indicative of high crystalline perfection.

High-resolution TEM (HR-TEM) was performed on these samples to verify the presence of extended-chain PAN. Figure 5 shows these microscopy images, where two coated SWNT bundles are imaged. On the basis of a comparison of panels a and b in Figure 5, it is clear that before and after electron beam exposure the PAN polymer coating is severely damage due to irradiation. Lattice images for the PAN polymer is observed at an average spacing of ~0.52 nm (Figure 5c,d), confirming that the tubular coating does consist of extended-chain polymer.

Similar tubular coating of PAN on SWNT has been previously observed in gel-spun fibers with high strength and modulus.[5] It was shown by high-resolution transmission electron microscopy that this tubular coating of PAN consists of extended-chain PAN molecules, where lattice spacing of 0.52 nm was observed.[5] In addition, X-ray diffraction for these fibers also showed the presence of more planar zigzag segments in the PAN-chain conformation, further indicating the presence of extended-chain PAN.[5]

On the basis of Table 1 and Figure 2, it was also found that a higher concentration of PAN was required as compared to the

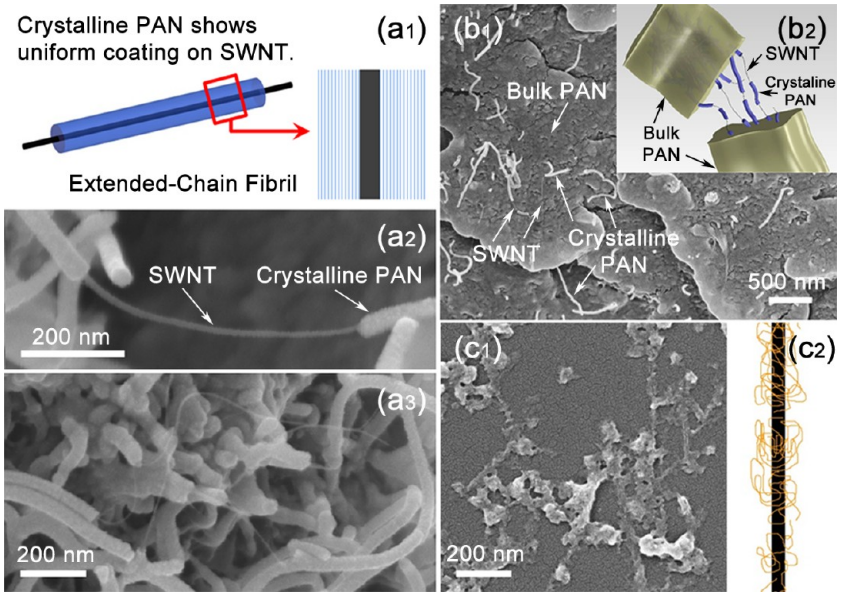

Figure 4. (a_1) Schematic of PAN tubular coating consisting of extended-chain crystals. (a_2 and a_3) SEM images of the crystalline PAN at the interphase in the vicinity of SWNT. (b_1) SEM image of a fractured surface of a PAN/SWNT composite film showing the tubular PAN coating at the interphase is distinct from the bulk region of PAN polymer and (b_2) corresponding schematic. (c_1) SEM image and (c_2) schematic of the solution ($S\text{-}a_2$) samples processed at lower concentration.

dx.doi.org/10.1021/am302382m | ACS Appl. Mater. Interfaces 2013, 5, 807−814

Table 2. Wide-Angle X-ray PAN (*hkl*) Indexing, *d*-Spacing, and Crystal Size Information for Each PAN/SWNT Sample[a]

		WAXD crystal plane						
		(200)	(110)	(310)	(120)	(420)	(002) (graphite)	(100) (carbon)
(S-a) tubular PAN coating	2θ (deg)	16.7	17.3	29.3	31.7	45.5	26.2	43.2
	d-spacing (nm)	0.531	0.512	0.304	0.282	0.199	0.340	0.209
	crystal size (nm)	7.2	4.5	1.8	9.6	5.2	3.1	3.3
(S-b) kebab PAN coating	2θ (deg)	16.9		29.4			26.0	42.8
	d-spacing (nm)	0.526		0.303			0.343	0.211
	crystal size (nm)	5.8		2.1			2.7	3.0
(S-c) irregular PAN coating	2θ (deg)	16.7		28			25.8	42.5
	d-spacing (nm)	0.531		0.318			0.346	0.213
	crystal size (nm)	5.4		2.5			2.9	2.5
as-received SWNT	2θ (deg)						26.2	43.1
	d-spacing (nm)						0.340	0.210
	crystal size (nm)						2.9	3.4

[a]Information for the two carbon peaks observed is also listed.

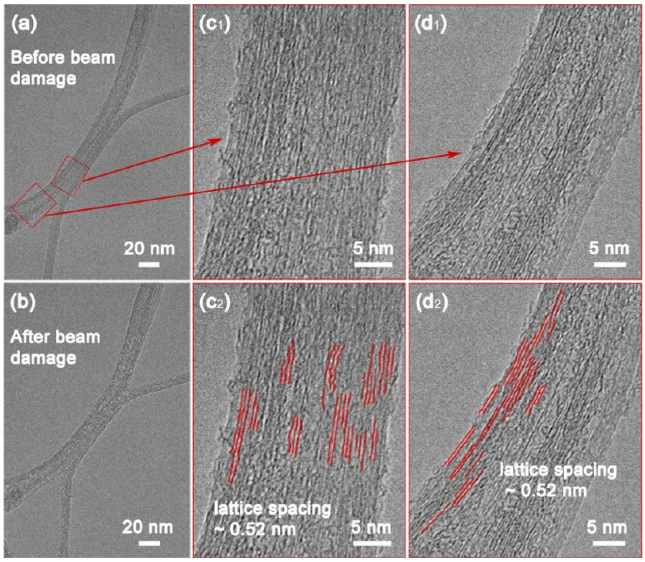

Figure 5. High-resolution transmission electron micrographs of (S-a) tubular coated PAN/SWNT samples. (a) Shows the samples at the onset of electron beam exposure and (b) shows the samples after ~5 min of beam exposure. (c_1 and d_1) Show two areas of the PAN/SWNT sample where the PAN lattice of ~0.52 nm is observed (Note: images are taken before beam damage at 5 min). For c_2 and d_2, a schematic of the lattice observations is provided.

concentration needed to form folded-chain (kebab) PAN crystals. The mechanism for fibrillar crystallization under shear requires that the nuclei form from extended-chain polymer molecules. The polymer molecules become extended when normal shear forces act on the chain during extensional flow within the stream-lines of the solution. These forces become more pronounced as the polymer concentration is increased.

For comparison, low concentration solutions (S-a_2) were subjected to the same procedure as S-a_1. In this case, the PAN polymer was not able to maintain a similar tubular coating on the SWNT. The PAN polymer can be seen to clearly wrap onto the SWNT bundles (Figure 4c_1,c_2), but there is a fair amount of dewetting and globular formation. While at low concentration the polymer molecules do undergo extensional forces under shear, entropic forces also act on the chains causing the molecules to recoil. At lower polymer concentrations, the extension-coiling transition of the polymer chain is less stable and faster. For this reason, the formation of the extended-chain nuclei needed for fibrillar growth shows a concentration dependence. At higher polymer concentration, the extensional forces will be larger and the entropic recoiling of the polymer is delayed due to the physical presence "crowding" of the other chains. Under these conditions, the SWNT is able to act as a more effective template for the extended-chain polymer to nucleate and support the crystal growth.

The uniform tubular coating with an average thickness on the order of ~43 nm (Figure 4a_1−a_3) was observed on SWNT bundles (~10 nm in diameter) in solution S-a_1. The average coating thickness (based on 60 measurements) of PAN on the SWNT was determined to be ~16.8 nm by SEM and ~5 to 12 nm by TEM. The difference in coating thickness may be due to the presence of metallic coating (i.e., Experimental Section) on the samples for SEM imaging. On the basis of WAXD, the crystal size perpendicular to the (200) plane (along the PAN chain-axis) is ~7.2 nm (Table 2), and this is consistent with TEM observations. The WAXD results along with the HR-TEM data (Figure 5) suggest that the tubular coating is almost entirely crystalline. Considering the similarity between SWNT and polymers, as suggested in previous studies,[42,43] the polymer chains easily interact with SWNT and nucleate and grow on SWNT surfaces. Since PAN does not crystallize as readily as other linear polymers, the presence of CNT is considered to largely contribute to lowering the barrier for PAN polymer fibrillar growth. The extended-chain conformation is the most preferred structure for strong fibers since it provides better chain alignment and minimizes the disordered regions.

By incorporating these procedures into composite processing steps, these specific crystallization conditions can be utilized to grow extended-chain PAN interfacial structures in the macroscopic system. PAN/SWNT dispersions were prepared using the S-a_1 procedure, and these coated SWNT are subsequently dispersed into a high concentration PAN solution in order to prepare a macroscopic composite. Figure 4b_1,b_2 shows a schematic and SEM image of a fractured surface (i.e., fractured during tensile test) for the PAN/SWNT film (0.5 wt % SWNT loading). It is clear that the interfacial polymer is distinctive as compared to the bulk polymer. It is also found that the highly crystalline interphase region due to its structural specificity (i.e., better ordering and orientation of polymer chains) behaves differently from the bulk polymer in the composite. The observed failure mechanisms of both systems are quite different, and this has also been observed by others.[5,7,44−46] The mechanical behavior and analysis of these polymer coated

SWNT in the overall composite is the subject of a future publication.

3.2. Hybrid Shish-Kebab Structure. The first observation of PAN (helical polymer) forming kebabs (lamellar crystals with folded-chain conformation) on SWNT shish (Figure 6a) is shown here. Investigations using electron microscopy indicate that, in dilute solutions (S-b), PAN kebabs preferentially form under quiescent and slow cooling (i.e., no shear during cooling) conditions (Figure 6b–d). WAXD 2θ versus intensity curves show PAN (200) and (310) peaks. As compared to the tubular coated PAN/SWNT, for the kebabs, only the major (200) peak is present, and this may be due to slightly lower crystalline perfection for the PAN kebabs. HR-TEM images for the PAN kebab crystals are not included due to the significant irradiation damage, which made image analysis challenging.

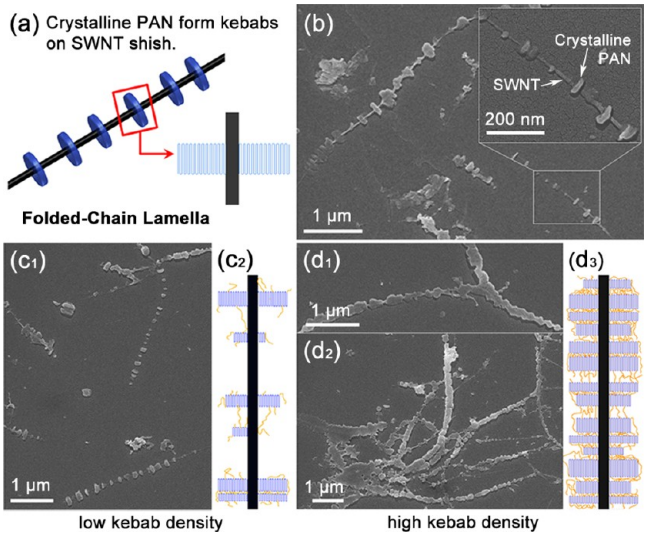

Figure 6. (a) Schematic of the interfacial crystalline structure of PAN kebabs (folded-chain crystals) formed on SWNT shish. (b) SEM images of PAN kebabs on SWNT. Schematic and SEM image of SWNT shish with (c_1 and c_2) low and (d_1, d_2, and d_3) high kebab densities.

Similar to the extended-chain PAN crystallization, the growth of polymer crystals on CNT is due to epitaxial interactions (i.e., a combination of lattice matching and geometrical confinement).[6,17] On the basis of SEM study, it was found that PAN kebabs did not form on every SWNT tube or bundle. In this work, it was found that statistical image analysis shows that the PAN kebabs grow on SWNT bundles with diameters ranging from 8 to 45 nm (average, ~28 nm). The irregularity also exists in lamellar size, and this may be due to frustrated (i.e., irregular) chain structures in the PAN folded-chain crystal as a result of the bulky nitrile side groups, which would induce large steric effects. This leads to PAN kebab density (lamellae sites per unit length of SWNT bundle) variations from SWNT bundle to bundle (Figure 6c,d). On the basis of 50 measurements, the average lamellar thickness of PAN kebabs is ~60 nm (maximum, ~121 nm; minimum, ~23 nm), and the average kebab density ranges from 3 to 17 μm^{-1} for low- (Figure 6c) and high-density (Figure 6d) regions. The variation in density measurements is also affected by kebabs merging into each other. At higher nuclei density (Figure 6d), kebabs eventually connect and merge with each other via tie chains emerging from the kebab surfaces. Epitaxial interactions between the macromolecules and the graphitic substrate are also influenced by the perfectness (i.e., lack of defects) of the graphitic structure.[39] Defective or disordered structure in the SWNT wall can interrupt lattice matching/registry and thus the

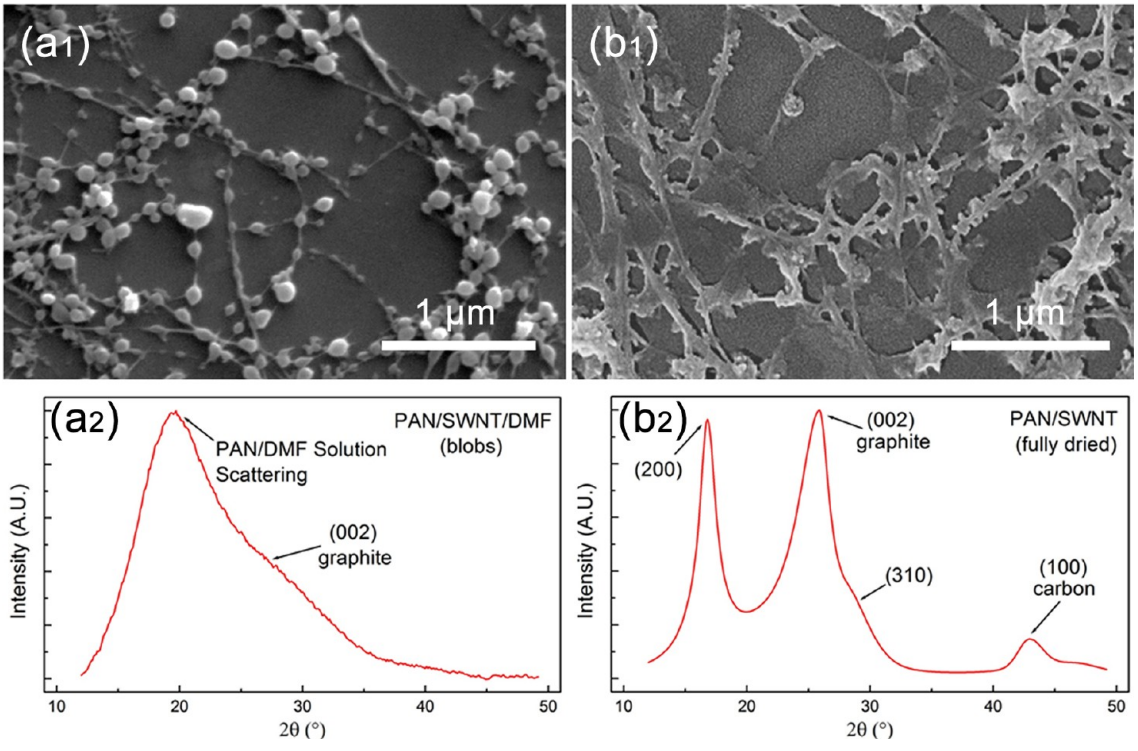

Figure 7. Scanning electron micrographs of S-c (a_1) PAN/SWNT/DMF blob and (b_1) fully dried PAN/SWNT samples. (a_2 and b_2) Wide-angle X-ray diffraction 2θ versus intensity profiles for the samples shown in a_1 and b_1, respectively.

epitaxial crystallization. The heterogeneity of SWNT samples in nature (i.e., bundle size, diameter, and graphitic structure) will influence the nucleation densities for PAN kebab growth.

3.2.1. Irregular Hybrid PAN/SWNT Crystal Growth. It was observed that, after quenching PAN/SWNT solution rapidly (S-c) followed by drying at room temperature (20 °C), the SWNT are coated by the globules or "blobs" (Figure $7a_1$). Once the samples are further dried used moderate heating (40−50 °C), the SWNT are coating with what appears to be irregular polymer crystalline lamellar (Figure $7b_1$). To understand these structures, WAXD is performed on both samples. It was found that the "blobs" are solvent rich, in that the X-ray pattern shows a large amorphous halo consistent with a polymer solution (Figure $7a_2$); there is a slight shoulder at 2θ ~26° coming from the carbon graphitic (002) peak (Figure $7a_2$). Upon further drying, all solvent is removed and "blob" structure has been transformed to irregular PAN lamellae (Figure $7b_1$). The X-ray profile displays several crystalline PAN peaks (Figure $7b_2$). The WAXD curve is almost identical to that of the PAN/SWNT hybrid kebab, where (200) and (310) PAN peaks are present. WAXD is unable to distinguish the regularity of the lamellar growth.

These observations provide some insight as to how crystalline PAN lamellae are formed along the CNT. The formation of these "blobs" is attributed to the dewetting of the PAN/DMF solution (i.e., liquid) coating on SWNT during the drying process. As mentioned earlier, at low PAN concentration, dewetting of the PAN is observed on SWNT. It should also be noted that the "blobs" form periodically along the SWNT axis. This may indicate the initial polymer interaction on the SWNT was epitaxial in nature (i.e., PAN polymer initially nucleated crystal growth at first interaction with the SWNT during sonication). As the DMF is subsequently removed during drying, the PAN is able to form crystalline domains as evidenced by X-ray diffraction (Figure $7b_2$).

4. CONCLUSIONS

In summary, this work provides insight toward control of the interfacial morphology formation by means of epitaxial crystallization. Control over the interfacial structure also indicates that the overall structural makeup of the nanocomposite is influenced by crystallization processes, where specific interfacial morphology formations in polymer/CNT composites dictate the macroscopic performance. In addition, for the same polymer system, completely different interphase morphologies were induced using slight changes in the crystallization procedures. This work brings to light the ability to control structural registry from the nano- to macroscale in nanocomposites as well as the specificity of the processing conditions for this to occur. The formation of polymer interfacial structure in polymer/nanotube composites is a key factor toward improving stress transfer between the polymer matrix and CNT fillers.

AUTHOR INFORMATION

Corresponding Author

*E-mail: m.minus@neu.edu.

Notes

The authors declare no competing financial interest.

ACKNOWLEDGMENTS

The authors express their sincere thanks to the Air Force Office of Scientific Research (AFOSR) (FA9550-11-1-0153) for financial support of this work.

REFERENCES

(1) Baughman, R. H.; Zakhidov, A. A.; de Heer, W. A. *Science* **2002**, *297*, 787−792.
(2) Treacy, M. M. J.; Ebbesen, T. W.; Gibson, J. M. *Nature* **1996**, *381*, 678−680.
(3) Wong, E. W.; Sheehan, P. E.; Lieber, C. M. *Science* **1997**, *277*, 1971−1975.
(4) Chae, H. G.; Choi, Y. H.; Minus, M. L.; Kumar, S. *Compos. Sci. Technol.* **2009**, *69*, 406−413.
(5) Chae, H. G.; Minus, M. L.; Kumar, S. *Polymer* **2006**, *47*, 3494−3504.
(6) Minus, M. L.; Chae, H. G.; Kumar, S. *Polymer* **2006**, *47*, 3705−3710.
(7) Minus, M. L.; Chae, H. G.; Kumar, S. *Macromol. Chem. Phys.* **2009**, *210*, 1799−1808.
(8) Jiang, L. Y.; Tan, H. L.; Wu, J.; Huang, Y. G.; Hwang, K. C. *Nano* **2007**, *2*, 139−148.
(9) Coleman, J. N.; Cadek, M.; Ryan, K. P.; Fonseca, A.; Nagy, J. B.; Blau, W. J.; Ferreira, M. S. *Polymer* **2006**, *47*, 8556−8561.
(10) Lourie, O.; Wagner, H. D. *Appl. Phys. Lett.* **1998**, *73*, 3527−3529.
(11) Tsuda, T.; Ogasawara, T.; Deng, F.; Takeda, N. *Compos. Sci. Technol.* **2011**, *71*, 1295−1300.
(12) Wernik, J. M.; Cornwell-Mott, B. J.; Meguid, S. A. *Int. J. Solids Struct.* **2012**, *49*, 1852−1863.
(13) Schadler, L. *Nat. Mater.* **2007**, *6*, 257−258.
(14) Schadler, L. S.; Brinson, L. C.; Sawyer, W. G. *JOM* **2007**, *59*, 53−60.
(15) Chae, H. G.; Minus, M. L.; Rasheed, A.; Kumar, S. *Polymer* **2007**, *48*, 3781−3789.
(16) He, L. H.; Zheng, X. L.; Xu, Q.; Chen, Z. M.; Fu, J. W. *Appl. Surf. Sci.* **2012**, *258*, 4614−4623.
(17) Li, C. Y.; Li, L.; Cai, W.; Kodjie, S. L.; Tenneti, K. K. *Adv. Mater.* **2005**, *17*, 1198−1202.
(18) Minus, M. L.; Chae, H. G.; Kumar, S. *ACS Appl. Mater. Interfaces* **2012**, *4*, 326−330.
(19) Zhang, L.; Tao, T.; Li, C. *Polymer* **2009**, *50*, 3835−3840.
(20) Zhang, S.; Lin, W.; Wong, C.-P.; Bucknall, D. G.; Kumar, S. *ACS Appl. Mater. Interfaces* **2010**, *2*, 1642−1647.
(21) Zhang, F.; Zhang, H.; Zhang, Z.; Chen, Z.; Xu, Q. *Macromolecules* **2008**, *41*, 4519−4523.
(22) Garcia-Gutierrez, M. C.; Hernandez, J. J.; Nogales, A.; Pantine, P.; Rueda, D. R.; Ezquerra, T. A. *Macromolecules* **2008**, *41*, 844−851.
(23) Hernández, J. J.; García-Gutiérrez, M.-C.; Rueda, D. R.; Ezquerra, T. A.; Davies, R. J. *Compos. Sci. Technol.* **2012**, *72*, 421−427.
(24) Yoshioka, T.; Tsuji, M.; Kawahara, Y.; Kohjiya, S.; Manabe, N.; Yokota, Y. *Polymer* **2005**, *46*, 4987−4990.
(25) Ning, N.; Zhang, W.; Zhao, Y.; Tang, C.; Yang, M.; Fu, Q. *Polymer* **2012**, *53*, 4553−4559.
(26) Li, B.; Li, L. Y.; Wang, B. B.; Li, C. Y. *Nat. Nanotechnol.* **2009**, *4*, 358−362.
(27) Imase, T.; Ohira, A.; Okoshi, K.; Sano, N.; Kawauchi, S.; Watanabe, J.; Kunitake, M. *Macromolecules* **2003**, *36*, 1865−1869.
(28) Sano, M.; Sandberg, M. O.; Yoshimura, S. *Langmuir* **1994**, *10*, 3815−3819.
(29) Tracz, A.; Jeszka, J. K.; Kucinska, I.; Chapel, J. P.; Boiteux, G.; Kryszewski, M. *J. Appl. Polym. Sci.* **2002**, *86*, 1329−1336.
(30) Tuinstra, F.; Baer, E. *J. Polym. Sci., Part B: Polym. Lett.* **1970**, *8*, 861−865.
(31) Cheng, S.; Chen, X.; Hsuan, Y. G.; Li, C. Y. *Macromolecules* **2012**, *45*, 993−1000.
(32) Dean, D. M.; Rebenfeld, L.; Register, R. A.; Hsiao, B. S. *J. Mater. Sci.* **1998**, *33*, 4797−4812.

(33) Vancso, G.; Liu, G.; Karger-Kocsis, J.; Varga, J. *Colloid Polym. Sci.* **1997**, *275*, 181−186.
(34) Haggenmueller, R.; Fischer, J. E.; Winey, K. I. *Macromolecules* **2006**, *39*, 2964−2971.
(35) Zhang, S.; Minus, M. L.; Zhu, L. B.; Wong, C. P.; Kumar, S. *Polymer* **2008**, *49*, 1356−1364.
(36) Hoffman, J. D. *Polymer* **1979**, *20*, 1071−1077.
(37) Pennings, A.; Kiel, A. *Colloid Polym. Sci.* **1965**, *205*, 160−162.
(38) Sakurada, I.; Ito, T.; Nakamae, K. *J. Polym. Sci., Part C: Polym. Symp.* **1967**, *15*, 75−91.
(39) Wittmann, J. C.; Lotz, B. *Prog. Polym. Sci.* **1990**, *15*, 909−948.
(40) Holland, V. F.; Mitchell, S. B.; Hunter, W. L.; Lindenmeyer, P. H. *J. Polym. Sci.* **1962**, *62*, 145−151.
(41) Stefani, R.; Chevereton, M.; Garnier, M.; Eyraud, C. *Compt. Rend.* **1960**, *251*, 2174.
(42) Zhang, S. J.; Kumar, S. *Small* **2008**, *4*, 1270−1283.
(43) Green, M. J.; Behabtu, N.; Pasquali, M.; Adams, W. W. *Polymer* **2009**, *50*, 4979−4997.
(44) Coleman, J. N.; Khan, U.; Blau, W. J.; Gun'ko, Y. K. *Carbon* **2006**, *44*, 1624−1652.
(45) Coleman, J. N.; Cadek, M.; Blake, R.; Nicolosi, V.; Ryan, K. P.; Belton, C.; Fonseca, A.; Nagy, J. B.; Gun'ko, Y. K.; Blau, W. J. *Adv. Funct. Mater.* **2004**, *14*, 791−798.
(46) Song, K.; Zhang, Y.; Meng, J.; Minus, M. L. *J. Appl. Polym. Sci.* **2012**, *127*, 2977−2982.